Proc. of the 9th International Symposium on Geotechnical Safety and Risk (ISGSR)
Edited by Zhongqiang Liu, Jian Dai and Kate Robinson
Published by Research Publishing, Singapore. ©2025 The Author(s), CC-BY 4.0 licence.
doi: 10.3850/GRF-25280825_isgsr-109-P356-cd

SEA LEVEL RISE EFFECTS ON EARTHQUAKE-INDUCED SOIL LIQUEFACTION

Meera L. Kota[1], Scott J. Brandenberg[2], Margit Maple[3], Timu Gallien[4]

[1] Civil and Environmental Engineering, University of California, Los Angeles, 5731 Boelter Hall, USA
E-mail: meerakota@g.ucla.edu
[2] Civil and Environmental Engineering, University of California, Los Angeles, 5731 Boelter Hall, USA
E-mail: sjbrandenberg@g.ucla.edu
[3] Civil and Environmental Engineering, University of California, Los Angeles, 5731 Boelter Hall, USA
E-mail: margitmaple@gmail.com
[4] Civil and Environmental Engineering, University of California, Los Angeles, 5731 Boelter Hall, USA
E-mail: tgallien@seas.ucla.edu

1. Abstract

This paperpresents probabilistic liquefaction hazard analysis (PLHA)results for groundwater conditions associated with different sea level rise scenarios at an example site in southern California.Finite element simulations model groundwater conditions for various sea level rise scenarios, and the subsequent pore pressures are then used in a PLHA framework to compute the annual down-crossing rate of factor of safety. Two meters of sea level rise is found to cause a 4-fold increase in the annual probability of liquefaction triggering.
Keywords: liquefaction, sea level rise, seismic hazard, groundwater simulations, probabilistic analysis, climate change.

2. Introduction

Global sea levels are expected to rise between two to five meters by the year 2150 (Fox-Kemper et al., 2021).Coastal aquifers are highly dynamic groundwater systems controlled by opencoast and embayment water levels.The beach groundwater system is a shallow, unconfined aquifer consisting of the saturated zone, unsaturated zone, and capillary fringe. Sea level rise, tides, and waves significantly influence groundwater in coastal areas, causing groundwater overheightsand transient oscillations that maysignificantly extendinland when low permeability layers confine the aquifer. However, dynamic groundwater conditions are typically ignored in liquefaction evaluations. Generally,the groundwater table depth is measured at the time of a geotechnical site investigation and assumed to be hydrostatic and stationary. Liquefaction is then evaluated for susceptible layers using a triggering procedure that compares liquefaction resistance to earthquake ground shaking. Earthquake-induced liquefactionconsequences include lateral spreading, sediment ejecta, lateral flow, passive pressures increases in retaining structures, and differential settlements, which can disrupt infrastructure (Fig. 1). Transient groundwater dynamics may change future liquefaction vulnerability as currently unsaturated soils become saturated. However, a paucity of research considerssea level rise impacts on near coast liquefaction.

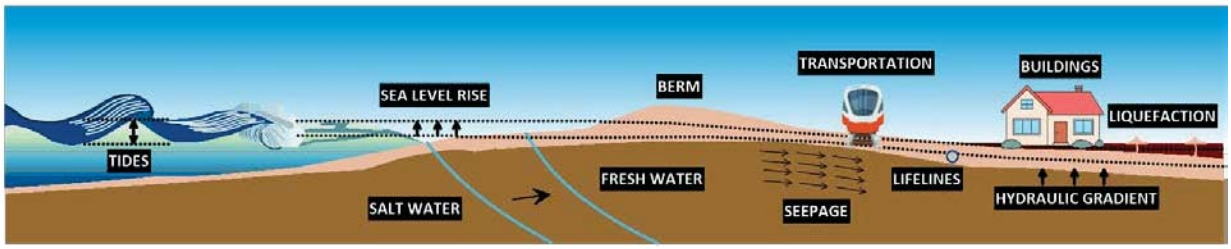

Fig. 1: Schematic outlining groundwater, sea level, and liquefaction interaction along the California coastline

3. Methodology

In this study, finite element simulations are used to computegroundwater conditions forced by tides and sea level rise. The resulting fluid pressures are combined with geotechnical conditions and earthquake shaking intensity in a probabilistic liquefaction hazard assessment (PLHA). An example analysis is performed atCardiff State Beach in Southern California. Cardiff State Beach is a 150 meter wide sand spit with beach groundwater experiencing tidal forcing from both San Elijo Lagoon Estuary to its east and the Pacific Ocean to its west. The estuary is connected to the ocean through a single, narrow (~ 30 m) inlet at its northwestern end. In the lagoon, the falling tide outflow is limited by the inlet channel and sillelevation (~1 m NAVD88). The tides are characterized as mixed semi-diurnal, with tidal ranges varying from 1.4 m during neap tides to 2.3 m during spring tides. From an infrastructure perspective, Highway 101 and the coastal Amtrak line lie to the east of the beach; additionally a parking lot is adjacent to the lagoon. The native beach sand is medium grained (D50 = 0.16 mm) and was nourished in 2012 with coarse sand (D50 = 0.57 mm) (Ludka et al., 2016). The beach remained

elevated above 2010 levels by about 1 m through January 2016, suggesting a retention of the nourishment layer, especially on the upper beach (Ludka et al., 2016).

3.1. Field Measurements

A digital terrain model (DTM) is constructed in the projected coordinate system WGS 1984 UTM Zone 11N and vertical datum NAVD88 m, with a grid size of 0.5 m. Beach topography was measured from the upper beach to 8m depth on 21 December 2015 using GPS-equipped platforms (Ludka et al., 2019). LiDAR is used to characterize stable back beach elevations (NOAA,2022). Road and lagoon elevations are augmented using recent high-resolution LIDAR (OCMP, 2022). In 2015-2016 16 pressure sensors measuring at 2 Hz were deployed along a cross-shore transect from the ocean to the estuary (Fig. 2B) to measure dynamic beach groundwater levels.One pressure sensor (P1) was placed in the estuary to monitor water levels.

3.2. 2-D Groundwater analysis

PFLOTRAN, an open-source multiphase groundwater flow model, is applied to Cardiff State Beach (Hammond et al., 2014). A 2D cross-shore transect is modeled as single phase using the Richard's equation without hysteresis, assuming a Darcy flux. The Richard's equation accounts for the influence of variable saturation on hydraulic conductivity (Richards, 1931). The Mualem formulation of the Van Genuchten equation is used to describe the flow, saturation, and permeability functions (Van Genuchten, 1980). In order to resolve rapidly variable beach topography, an explicit Voronoi polygon computational mesh is used. First, a Delauney triangular mesh is created using Triangle (Shewchuk, 1996). The resulting vertices are then used as centroids for the Voronoi mesh generated with LaGrit (LaGriT, 2023) (Figure 2A). Modeled pore pressures converged for Delauney triangular mesh sizes of 0.05 m^2 and finer; accordingly, this cell size constraint is used.

The model domain is created along a cross-shore transect following pressure sensor locations, extending from the shoreline over the San Elijo Lagoon 250 m inland(Fig.2C). The bottom of the domain is set as a no-flow boundary at -20m NAVD88. The seaward boundary and the beach face up to the crest of the sand spit are set to a hydrostatic seepage condition. This assumes a hydrostatic distribution of the boundary forcing pressure and only admits flow into the domain when the boundary pressure is above atmospheric. The top boundary inland from the crest of the sand spit is set to a conductance boundary condition, which is designed to mimic a lower permeability soil layer (Fig. 2C). This is similar to the seepage condition, except that a conductance parameter (permeability/distance) is specified instead of using boundary grid cell parameters. This allows for tuning of infiltration rates into the aquifer to account for lower permeability estuarine deposits. The inland (right) boundary is set as a no-flow boundary(Figure 2C).Marine boundaries are forced by converting water levels to hydrostatic pressure distributions. The water level applied at the ocean-side boundary is equal to the mean runup elevation calculated using NOAA observed water levels and wave measurements recorded at 10 m ocean depth (NOAA, 2024). Mean runup elevation is calculated using empirical formulae presented by Stockdon et al. (2006) as shown in Eq. (1) and assuming a Rayleigh distribution of wave runup:

$$R_{2\%} = 1.1\left(0.35\beta_f\sqrt{H_0 L_0}\right) + \frac{\sqrt{H_0 L_0\left(0.563\beta_f^2 + 0.004\right)}}{4.4} \quad (1)$$

where $^2{}_f$ is foreshore beach slope [-], H_0 is deep water significant wave height [m], and L_0 is deep water wavelength [m]. The estuary and inland boundary are forced using estuary water levels measured at P1. Sea level rise scenarios are considered by increasing all forcing water levels by1.0mand 2.0m.

A Newton solver is used with an absolute tolerance of $1x10^{-12}$ and a maximum of 50 iterations allowed. A maximum time step of 15 minutes is used in order to capture minimum and maximum water levels across the approximately 12-hour tidal cycles. The model is calibrated with respect to hydraulic conductivity (K); all other physical parameters were set to values typical for sandy beaches. Calibration of K is evaluated by minimizing overall RMSE of modeled pore pressure relative to in situ measurements. Regions of distinct soil characteristics, such as the constructed parking lot and larger grain size nourishment layer, are assigned unique hydraulic conductivity values (Fig.2C). Estuary borehole measurements found a clay/silt layer extending up to 9 ft (2.74 m) from the surface (AECOM, 2016). Therefore, an additional low permeability region is defined under the estuary extending to 0 m NAVD88 in order to represent the lagoon sediment deposits (Fig. 2C). A low hydraulic conductivity (1.0×10^{-13} m/s) is used for this region, essentially representing confined aquifer conditions. The conductance parameter for the boundary is also set to 1.0×10^{-13} m s^{-1} / m . The model is run using observationsfrom November and December of 2015. Model results are used to create CDFs of pore pressure at 150 m inland location. Pore pressure values are then applied as inputs to the liquefaction hazard assessment.

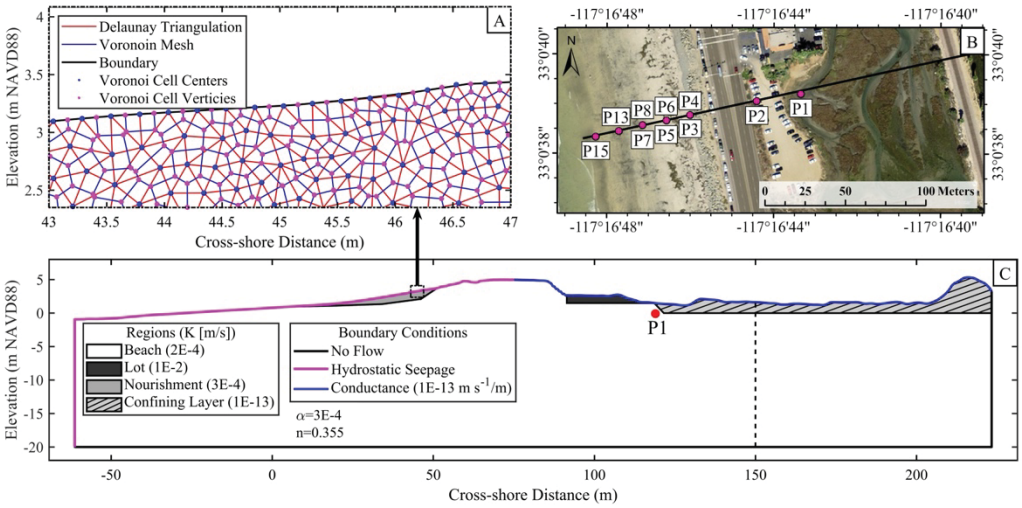

Fig. 2: A) Features used in development of explicit Voronoi polygon computational mesh. B) Buried pressure sensor array at Cardiff State Beach from winter of 2015. Black line is modelled cross-shore transect. C) PFLOTRAN model schematic of regions and boundary conditions. Estuary water levels measured at P1. Box indicates illustrated mesh extent. Liquefaction hazard analysis performed at x=150m.

3.3. Probabilistic Liquefaction Hazard Analysis

PLHA extends probabilistic seismic hazard analysis (PSHA) by integrating ground motion hazard with liquefaction hazard, and computes the annual rate of factor of safety against liquefaction dropping below a specified threshold. The general form of the PLHA solution is shown in Eq (1), where$\Lambda(FS_L < fs_l)$ is the annual rate of factor of safety against liquefaction, FS_L, dropping below a threshold value, fs_l, $n_{sources}$ is the number of earthquake fault rupture scenarios, $\lambda(M_i > m_{\min})$ is the rate of earthquakes of magnitude M larger than a minimum considered value, m_{min}, m_{max} is the maximum considered magnitude, r_{max} is the maximum considered distance, im is a ground motion intensity measure, m is magnitude, ξ is an array of variables used to define the soil properties and stress conditions used in a particular liquefaction triggering model, and r is distance. Solving Eq. 2 for many different values of fs_l results in a liquefaction hazard curve representing the annual downcrossing rate of fs_l.

$$\lambda(FS_L < fs_l) = \sum_{i=1}^{n_{sources}} \lambda(M_i > m_{\min}) \int_{m_{min}}^{m_{max}} \int_{0}^{r_{max}} \int_{-\infty}^{+\infty} P(FS_L < fs_l | im, m, \xi) f(im|m,r) f(r) f(m)\, dim\, dr\, dm \quad (2)$$

Within Eq. (2), $P(FS_L < fs_l|im, m, \xi)$ represents a probabilistic liquefaction triggering model, and $f(im|m,r)$represents a ground motion model. Ground motion uncertainty, and liquefaction triggering conditioned on ground motion are therefore both considered in PLHA. Here we, adopt the probabilistic triggering model proposedbyIdriss and Boulanger (2012), Cetin et al. (2014), Cetin et al. (2018), and ground motion model proposed by Boore et al. (2014). Fault sources are modelled using the Uniform California Earthquake Rupture Forecast (UCERF3) (Field et al., 2014). Calculations were implemented using a custom Python script using vectorised operations for computing source-to-site distance, ground motion intensity, and liquefaction resistance. Sample values were chosen for this site and are given as: fines content FC = 0, fines- and overburden-corrected SPT blow count, $(N_1)_{60} = 20$, vertical total stress$\sigma_v = 70\ kPA$, vertical effective stress $\sigma_v{}' = 70\ kPA$, time-averaged shear wave velocity in the upper 12m and 30m, $VS_{12} = 150\ {}^{m}/_{s}andVS_{30} = 250\ {}^{m}/_{s}$, respectively.PSHA and PLHA results are provided in Fig. 3 for mean sea level rise scenarios of 0m, 1m, and 2m relative to present day. Annual rates of non-exceedance of fs_l= 1 for the 0m, 1m, and 2m sea level rise scenarios are 0.0014 yr^{-1}, 0.0029 yr^{-1}, and 0.0057 yr^{-1}, respectively, which corresponds to return periods of 714, 345, and 175 years, respectively. Results suggest that 1m of sea level rise approximately doubles the liquefaction hazard, while 2m of sea level rise results in a 4-fold liquefaction hazard increase.

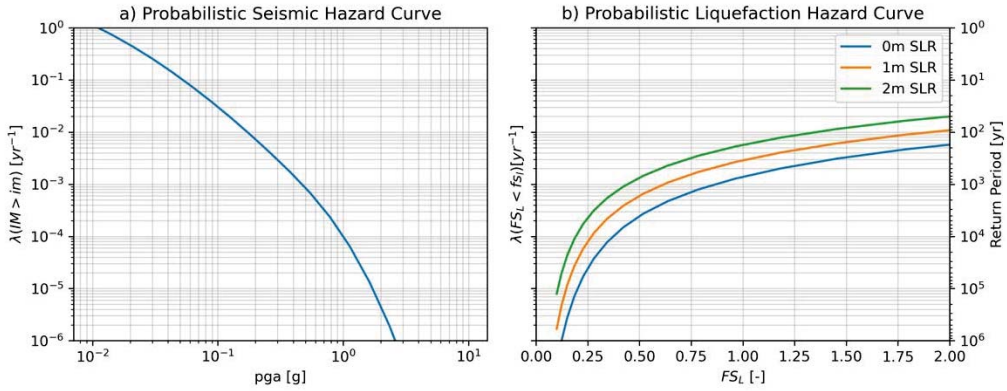

Fig. 3: Hazard curves for Cardiff State Beach: (a) PSHA and (b) PLHA

4. Conclusions and Future Work

Preliminary results suggest sea level rise will significantly impact liquefaction triggering hazard in the future. Additional geotechnical site investigations, hydraulic conductivity information, ground motion models, and liquefaction models will be required to make stronger conclusions. Liquefaction hazard sensitivity to temporally variable groundwater conditions also requires further investigation. Here, liquefaction's infrastructure impacts are neglected. Future ground deformation modelling is required to evaluate liquefaction effects. This work is part of a larger study evaluating SLR impacts on coastal liquefaction hazards throughout California.

Acknowledgements This research is funded by the University of California through The California Climate Action Grants under Application ID R02CP7031. We thank our collaborators from the California Geologic Survey, the United States Geologic Survey, and the California Seismic Safety Commission.

References

AECOM (2016). Environmental impact report / environmental impact statement for the sanelijolagoon restoration project. Technical report, San Elijo Lagoon Conservancy.

Boore, D., Stewart, J., Seyhan, E., and Atkinson, G. (2014). NGA-West2 equations for predicting PGA, PGV, and 5% damped PSA for shallow crustal earthquakes. *Earthquake Spectra*, 30:1057–1085.

Cetin, K. O., Seed, R. B., Kayen, R. E., Moss, R. E., Bilge, H. T., Ilgac, M., and Chowdhury, K. (2018). The use of the SPT-based seismic soil liquefaction triggering evaluation methodology in engineering hazard assessments. *MethodsX*, 5:1556–1575.

Field, E. H., Arrowsmith, R. J., Biasi, G. P., Bird, P., Dawson, T. E., Felzer, K. R., Jackson, D. D., Johnson, K. M., Thomas H. Jordan, C. M., Michael, A. J., Milner, K. R., Page, M. T., Parsons, T., Powers, P. M., Shaw, B. E., Thatcher, W. R., Weldon, R. J., and Zeng, Y. (2014). Uniform california earthquake rupture forecast, version 3 (ucerf3)—the time-independent model. *Bulletin of the Seismological Society of America 2014*, 104(3):1122–1180.

Fox-Kemper, B., Hewitt, H., Xiao, C., Adalgeirsdottir, G., Drijfhout, S., Edwards, T., Golledge, N., Hemer, M., Kopp, R., Krinner, G., Mix, A., Notz, D., Nowicki, S., Nurhati, I., Ruiz, L., Sallee, J.-B., Slangen, A., and Yu, Y. (2021). Ocean, cryosphere and sea level change. In *In Climate Change 2021: The Physical Science Basis. Contribution of Working Group I to the Sixth Assessment Report of the Intergovernmental Panel on Climate Change*. Cambridge University Press, Cambridge, United Kingdom and New York, NY, USA, pp. 1211–1362.

Hammond, G. E., Lichtner, P. C., and Mills, R. (2014). Evaluating the performance of parallelsubsurface simulators: An illustrative example with pflotran. Water resources research,50(1):208–228.

Kramer, S. L. and Mayfield, R. T. (2007). Return period of soil liquefaction. *Journal of Geotechnical and Geoenvironmental Engineering*, 133(7):802–813.

LaGriT (2023). Los alamos grid toolbox.

Ludka, B. C., Gallien, T., Crosby, S. C., and Guza, R. T. (2016). Mid-elnino erosion at nourished and unnourished southern california beaches. Geophysical Research Letters, 43(9):4510–4516.

Ludka, B. C., Guza, R., O'reilly, W., Merrifield, M., Flick, R., Bak, A. S., Hesser, T., Bucciarelli,R., Olfe, C., Woodward, B., et al. (2019). Sixteen years of bathymetry and waves at sandiegobeaches. Scientific data, 6(1):161.

Ninyo and Moore (1998). Geotechnical evaluation Coastal Protection Project Highway 101 Encinitas, California. Technical report, Ninyo and Moore Geotechnical and Environmental Sciences Consultants.

NOAA (2024a). 9410230 la jolla, ca - noaa tides currents.

NOAA (2024b). National tidal datum epoch.

Richards, L. A. (1931). Capillary conduction of liquids through porous mediums. physics,1(5):318–333.

Shewchuk, J. R. (1996). Triangle: Engineering a 2D Quality Mesh Generator and DelaunayTriangulator. In Lin, M. C. and Manocha, D., editors, Applied Computational Geometry, pages203–222. Springer-Verlag.

Stockdon, H. F., Holman, R. A., Howd, P. A., and Sallenger Jr, A. H. (2006). Empiricalparameterization of setup, swash, and runup. Coastal engineering, 53(7):573–588.

Van Genuchten, M. T. (1980). A closed-form equation for predicting the hydraulic conductivity ofunsaturated soils. Soil science society of America journal, 44(5):892–898.